Molecular Crystals and Liquid Crystals
Publication details, including instructions for authors and subscription information:
http://www.tandfonline.com/loi/gmcl20

Enhancing Efficiency of Dye-Sensitized Solar Cells Using TiO_2 Composite Films and RF-Sputtered Passivating Layer

Chang Hyo Lee [a], Kyung Hwan Kim [a] & Hyung Wook Choi [a]
[a] Department of Electrical Engineering, Kyungwon University, Gyeonggi-do, Korea
Version of record first published: 17 Sep 2012.

To cite this article: Chang Hyo Lee , Kyung Hwan Kim & Hyung Wook Choi (2012): Enhancing Efficiency of Dye-Sensitized Solar Cells Using TiO_2 Composite Films and RF-Sputtered Passivating Layer, Molecular Crystals and Liquid Crystals, 567:1, 9-18

To link to this article: http://dx.doi.org/10.1080/15421406.2012.702374

Mol. Cryst. Liq. Cryst., Vol. 567: pp. 9–18, 2012

ISSN: 1542-1406 print/1563-5287 online
DOI: 10.1080/15421406.2012.702374

Taylor & Francis
Taylor & Francis Group

Enhancing Efficiency of Dye-Sensitized Solar Cells Using TiO_2 Composite Films and RF-Sputtered Passivating Layer

CHANG HYO LEE, KYUNG HWAN KIM, AND HYUNG WOOK CHOI*

Department of Electrical Engineering, Kyungwon University, Gyeonggi-do, Korea

The aim of this work is to prevent the backtransfer of electrons due to direct contact between the electrolyte and the conductive substrate by using TiO_2 passivation. A thin TiO_2 passivating layer was deposited on a fluorine-doped tin oxide (*FTO) glass by radio frequency (RF) magnetron sputtering at different RF powers and substrate temperatures. A nanoporous TiO_2 nanoparticles/TiO_2 nanotubes (TNTs) upper layer was deposited by the screen-printing method on the TiO_2 passivating layer. The crystal structure and the morphology were characterized by X-ray diffraction (XRD) and a scanning electron microscope (SEM). The transmittance of TiO_2 films were characterized by ultraviolet–visible spectroscopy (UV-Vis). The conversion efficiency of a dye-sensitized solar cell (DSSC) was measured by a solar simulator (100 mW cm^{-2}). The thickness and the crystalline structure were adjusted by applying various working conditions, and the optical transmittance of the TiO_2 films depended on the morphology of the TiO_2 passivating layer. Using a TiO_2 passivating layer and a TiO_2/TNT hybrid electrode, the maximum conversion efficiency of the DSSC was measured to be 5.12%, due to the effective prevention of electron recombination to electrolyte. It was also found that the conversion efficiency of the DSSC was highly affected by the crystalline structure and thickness of the passivating layer.*

Keywords DSSCs; passivating-layer hydrothermal method; TiO_2 nanotube

Introduction

Dye-sensitized solar cells (DSSCs) have been studied intensively since their discovery in 1991 for use in a new generation of energy-harvesting devices because of their simple structure and functioning, low-cost fabrication, transparency, color control, and applicability in flexible DSSCs [1,2]. DSSCs have been studied extensively over the past few decades also as cheaper alternatives to silicon solar cells owing to their high-energy-conversion efficiency and low production cost [3,4]. DSSCs consist of a wide band-gap mesoporous metal oxide film, such as that of TiO_2, deposited on a conducting oxide layer as an electron transport layer; an organic dye as a sensitizer, such as ruthenium; an electrolyte as an ionic electron conductor, such as iodolyte; and a high work function metal as the counter

*Addressed correspondence to Hyung Wook Choi, Department of Electrical Engineering, Kyungwon University, San 65 Bokjeong-dong, Sujeong-gu, SeongNam, Gyeonggi-do 461-701, Korea (ROK). Tel.: +82-31-750-5562; Fax: +82-31-750-5491. E-mail: chw@kyungwon.ac.kr

electrode, such as platinum—i.e., DSSCs are composed of a dye-absorbed nanoporous TiO_2 layer on a conducting glass substrate, redox electrolytes, and a counter electrode. A unidirectional charge flow with no electron leakage at the interfaces is essential for high-energy conversion efficiency [5]. The energy conversion efficiency is likely to be dependent on the morphology and structure of the dye-adsorbed TiO_2 film. Grätzel et al. introduced mesoporous TiO_2 films as photoanodes to enhance the effective surface area to absorb more dye molecules and thus to achieve more light absorption and greater efficiency [6,7]. Subsequently, researchers started to explore the use of ordinal TiO_2 in DSSCs; this includes TiO_2 nanowires, nanorods, and TiO_2 nanotubes (TNTs). The high level of dye adsorption on TiO_2 in the form of nanorods and nanotubes is expected because of the high surface area of these nanostructures. The preparation of TNTs by a hydrothermal treatment of TiO_2 nanoparticle in a 10M NaOH aqueous solution has been reported [8,9]. In addition, to obtain high-performance DSSCs, it is desirable to prevent the carrier leakage at the nanoporous TiO_2/fluorine-doped tin oxide (FTO) interface by electron transfer to redox ions in the electrolyte [10]. To avoid this problem, a TiO_2 thin film is used as a compact layer in DSSCs [11]. During the last decade, many studies have been reported on the electrode modification of TiO_2. Some researchers have tried to prepare thin TiO_2 blocking (passivating) layers by dry processes, such as the sputtering method [12] and the chemical vapor deposition method [13], which are suitable for forming uniform and fine membranes over a large area with more stable material properties than those prepared using wet processes.

In this work, a thin TiO_2 passivating layer was deposited on an FTO glass by radio frequency (RF) magnetron sputtering at different RF powers and substrate temperatures. In addition, a nanoporous TiO_2 upper layer was prepared by an application of TNTs and TiO_2 nanoparticles constructed by the sol-gel method and the hydrothermal method.

Experimental Details

Deposition of TiO_2 Passivating Layer

To prevent the leakage caused by an electron transfer to the electrolyte, dense TiO_2 passivating layers were employed. Optically transparent conducting glass [FTO (fluorine-doped SnO_2, sheet resistance 8 Ω/sq)] was washed in ethanol and deionized (DI) water in an ultrasonic bath for 10 min. A passivating TiO_2 underlayer, 2″ in diameter and 0.25″ in thickness, with a purity of 99.99%, was deposited onto the FTO glass by sputtering with an RF magnetron at different RF powers (80 W, 120 W, 160 W, and 200 W) and substrate temperatures (room temperature, 200°C, 300°C, and 400°C). Argon gas was introduced into the chamber of the magnetron at 15 sccm at a working pressure of 5 mTorr for 1 h. The crystalline structure of the rutile-phase TiO_2 passivating layer was controlled by an increase in the working pressure at optimized constant conditions [14]. In order to remove the surface contaminants from the layer, presputtering was done for 20 min in pure argon.

Preparation of Electrode Films

The TiO_2 main layer was prepared using the sol-gel method. TNTs were prepared using a hydrothermal process described in the authors' previous work. TiO_2 particles, in the amount of 5 g, prepared by the sol-gel method, were mixed with 500 ml of a 10M NaOH aqueous solution, followed by hydrothermal treatment at 150°C (TNTs) in a Teflon-lined autoclave for 12 h. After the hydrothermal reaction, the treated nanoparticles were washed thoroughly

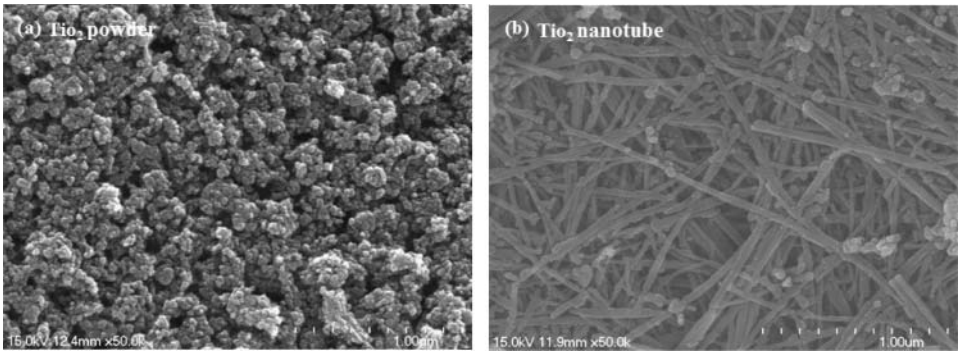

Figure 1. (a) FE-SEM images of the TiO_2 nanoparticles by the sol-gel method and (b) FE-SEM images of the TNTs films by the hydrothermal method at 150°C for 12 hours.

with DI water and 0.1M HCl and subsequently filtered and dried at 80°C for one day. To achieve the desired TNT size and crystallinity, the nanoparticles were calcined in air at 500°C for 1 h. Field emission scanning electron microscopy (FE-SEM) images of the TiO_2 nanopaticles and TNTs prepared by the sol-gel method at hydrothermal temperatures are shown in Fig. 1 [15]. TiO_2 nanoparticles and TNTs prepared by the sol-gel and hydrothermal methods were mixed at a specific weight ratio (TiO_2 nanoparticles: TNTs 9:1, 10 wt.%) and ground in a mortar. Acetic acid (1 ml), distilled water (5 ml), and ethanol (30 ml) were added gradually, drop by drop, to disperse the TiO_2 nanoparticles and TNTs under continuous grinding. The TiO_2 dispersions in the mortar were transferred with an excess of ethanol (100 ml) to a tall beaker and stirred with a 4-cm-long magnet tip at 300 rpm. Anhydrous terpineol (20 g) and ethyl celluloses (3 g) in ethanol were added, followed by further stirring. The dispersed contents were concentrated by evaporating the ethanol in a rotary evaporator. The pastes were finished by grinding in a three-roller mill [16]. A TiO_2 film with a thickness of 10 μm was deposited onto the pretreated conducting glass using the screen-printing technique and sintered again at 450°C for 15 min and at 500°C for 15 min in air.

Assembly of the Dye-Sensitized Solar Cells

The nanoporous TiO_2 electrode films were immersed in the dye (N719) complex for 24 h at room temperature. A counter electrode was prepared by spin-coating with an H_2PTCl_6 solution onto the FTO glass and heating at 450°C for 30 min. The dye-adsorbed TiO_2 electrode and the platinum counter electrode were assembled into a sandwich-type cell and sealed with a hot-melt sealant 50 μm thick. An electrolyte solution was introduced through a drilled hole in the counter electrode. The hole was then sealed using a cover glass.

Measurements

The TiO_2 passivating layer was measured by X-ray diffraction (XRD) using a Rigaku D/MAX-2200 diffractometer with CuKα radiation. The morphology and the thickness of the prepared TiO_2 passivating layers were investigated using FE-SEM (model S-4700, Hitachi). The transmittance of the TiO_2 thin films was measured using a UV-Visible spectrometer (UV-Vis 8453, Agilent). The conversion efficiency of the fabricated DSSC was measured

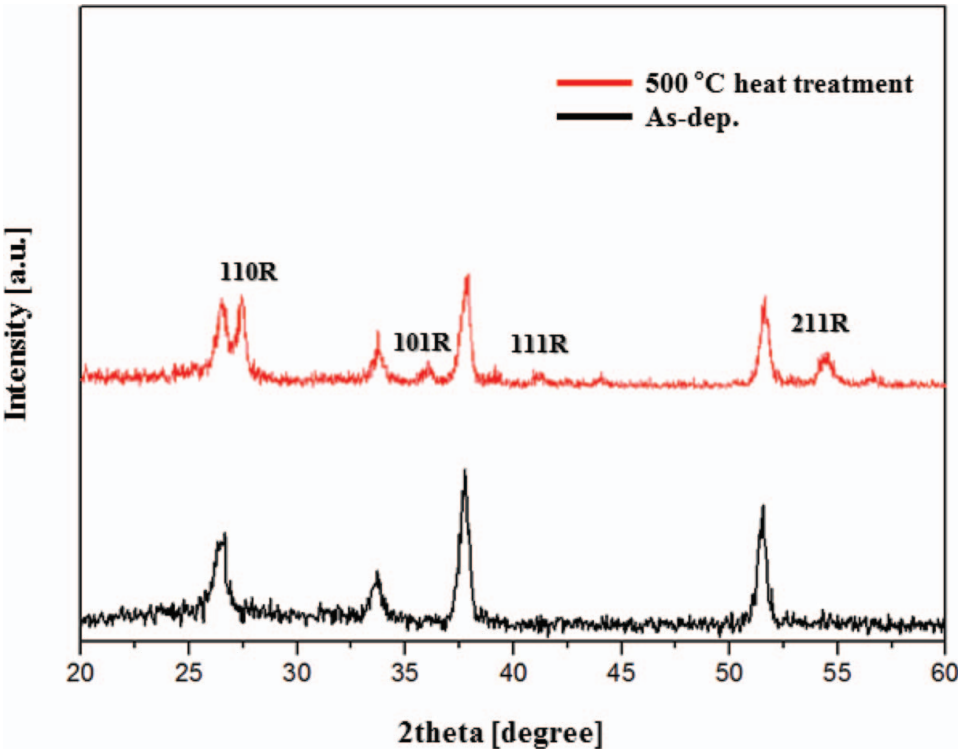

Figure 2. XRD patterns of as-deposited and annealed-deposited TiO_2 passivating layer.

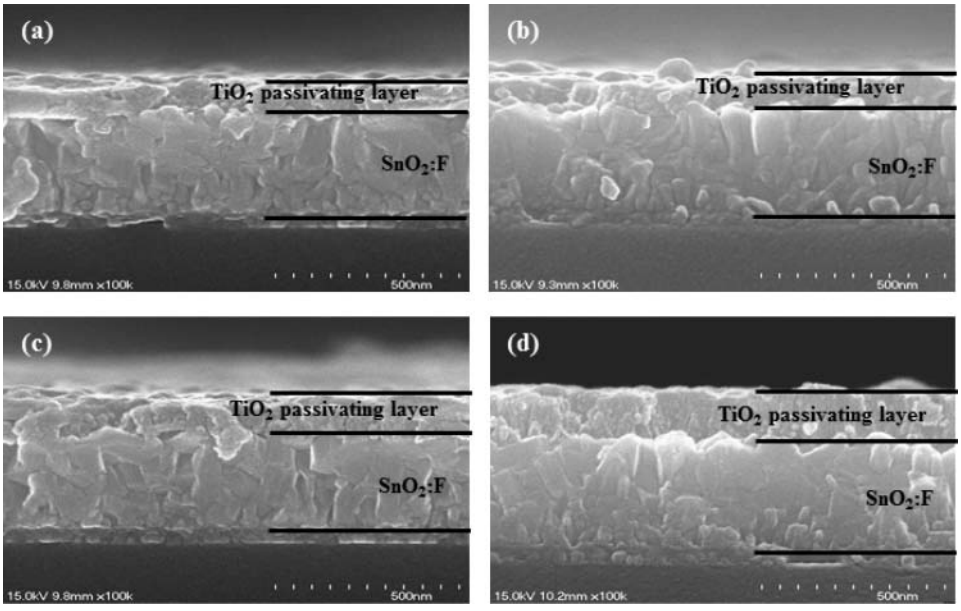

Figure 3. The cross-sectional FE-SEM image of the TiO_2 passivating layer at various RF powers: (a) 80 W, (b) 120 W, (c) 160 W, and (d) 200 W.

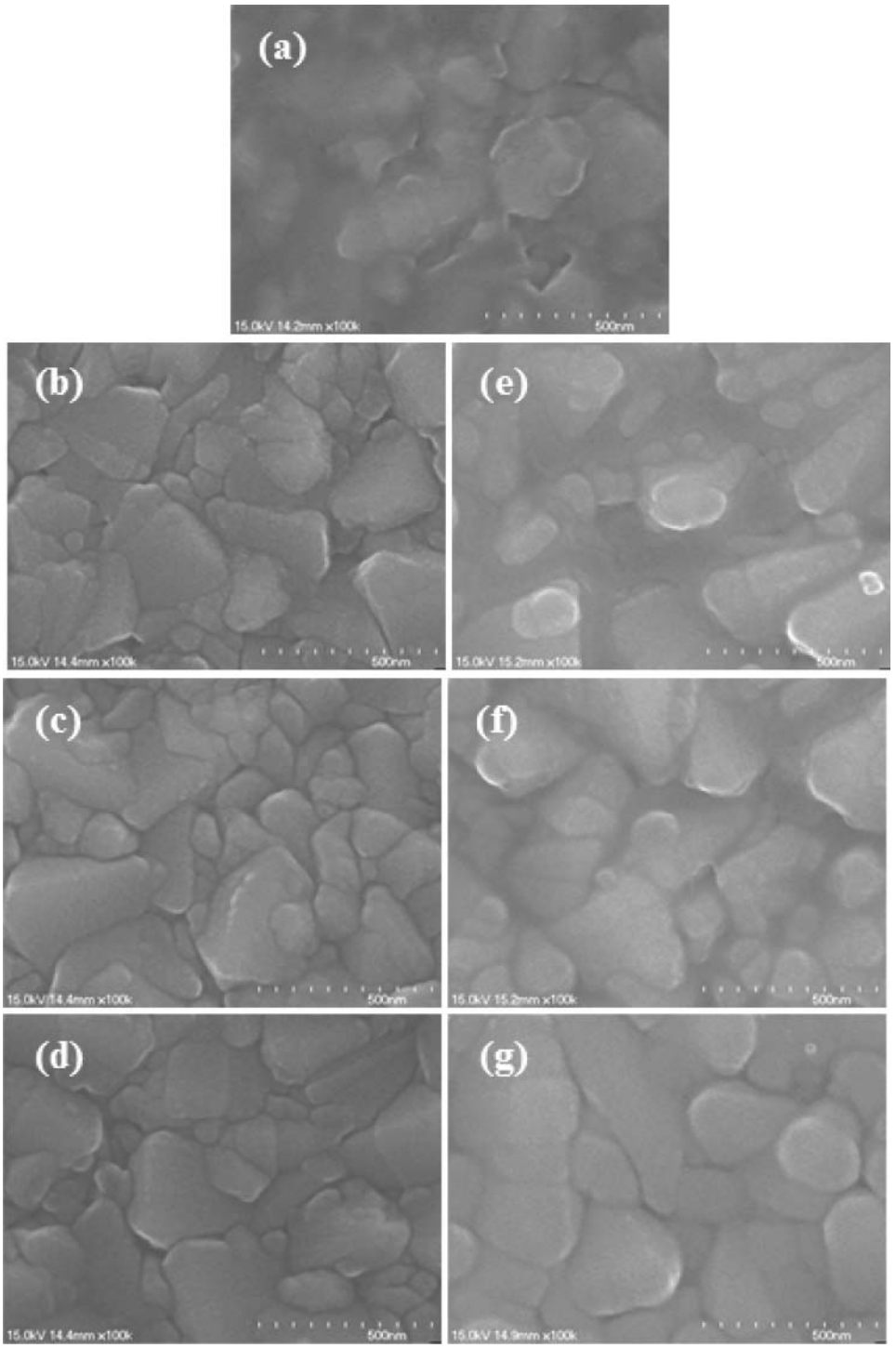

Figure 4. The FE-SEM images of the TiO_2 passivating layer deposited at various RF powers and substrate temperatures: (a) FTO, (b) 80 W, (c) 120 W, and (d) 160 W at room temperatures (e) 200°C, (f) 300°C, and (g) 400°C at RF power of 160 W.

using an I-V solar simulator (Solar Simulator, McScience). The active area of the resulting cell exposed to light was approximately 0.25 cm^2 (0.5 cm × 0.5 cm).

Results and Discussion

Figure 2 shows XRD patterns for the deposited TiO_2 passivating layer. As-deposited films are amorphous, and the observed peaks are due to the FTO backcontact. Films annealed at 450°C are crystalline and show evidence only of the rutile phase of TiO_2. These results are in agreement with literature data [14]. The XRD patterns of the TiO_2 passivating layer annealed at 450°C shows prominent rutile-phase peaks: 27.4° (110), 54.2° (211).

The cross-sectional FE-SEM image of the TiO_2 passivating layer is shown in Fig. 3. The cross-sectional view clearly indicates that it is composed of three parts. The top part is the TiO_2 passivating layer; the middle one is the FTO layer; and the lowest one is the glass substrate. It was shown that the deposition rate of the TiO_2 passivating layer monotonically increased with increasing RF power due to increase in the plasma density. Because the sputtering rate of Ar ions is critically dependent on the current density, which is applied on the cathode target, the sputtering rate of the TiO_2 passivating layer increased with increasing RF power [17]. Figure 3 shows the FE-SEM surface morphologies of the bare FTO substrate and the TiO_2 passivating layers.

The TiO_2 passivating layers deposited at low temperatures revealed rough surfaces, as shown in Fig. 4b, c, and d. Figure 4e, f, and g shows the increasing substrate temperatures, the changes from rough surface to smooth with the disappearance of the TiO_2 particles, which means that TiO_2 particles might be cohesive.

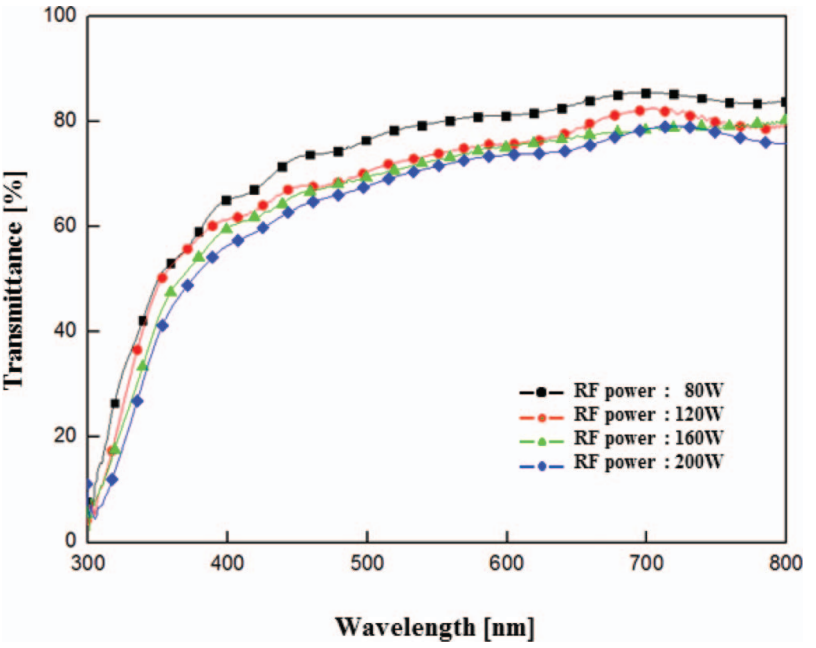

Figure 5. The optical transmittance of the TiO_2 passivating layer at the sputtering power.

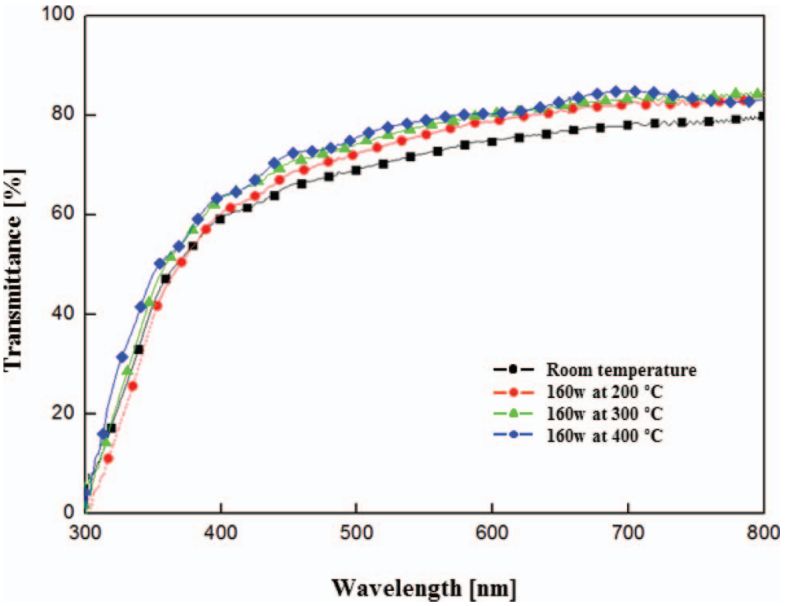

Figure 6. The optical transmittance of the TiO_2 passivating layer at sputtering room temperatures.

Figures 5 and 6 show the transmittance spectra of the TiO_2 passivating layer deposited by sputtering with the RF magnetron at different RF powers and substrate temperatures. From Fig. 5, the transmittance of the films is decreased by increasing the RF power. Considering the light transmission though the TiO_2/FTO/glass substrate, the RF

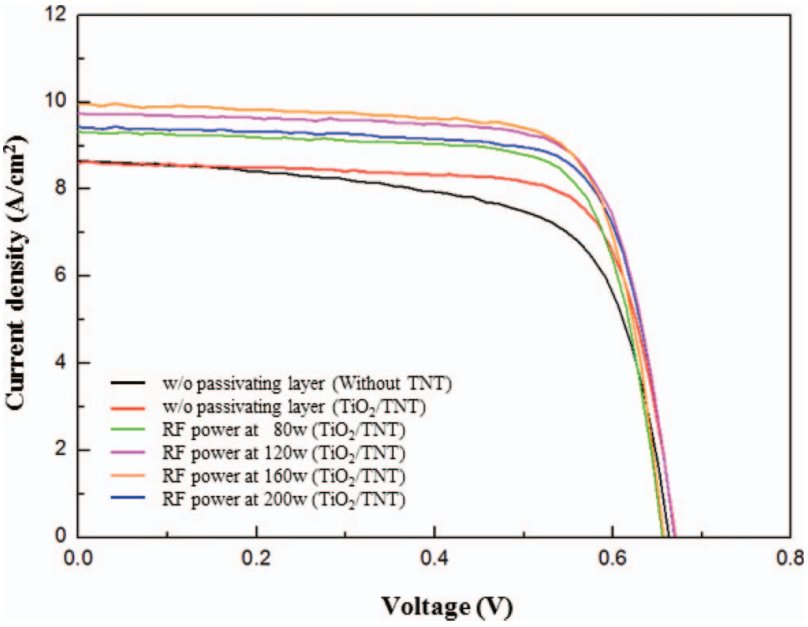

Figure 7. The photocurrent and voltage curves of the DSSCs prepared at the sputtering power.

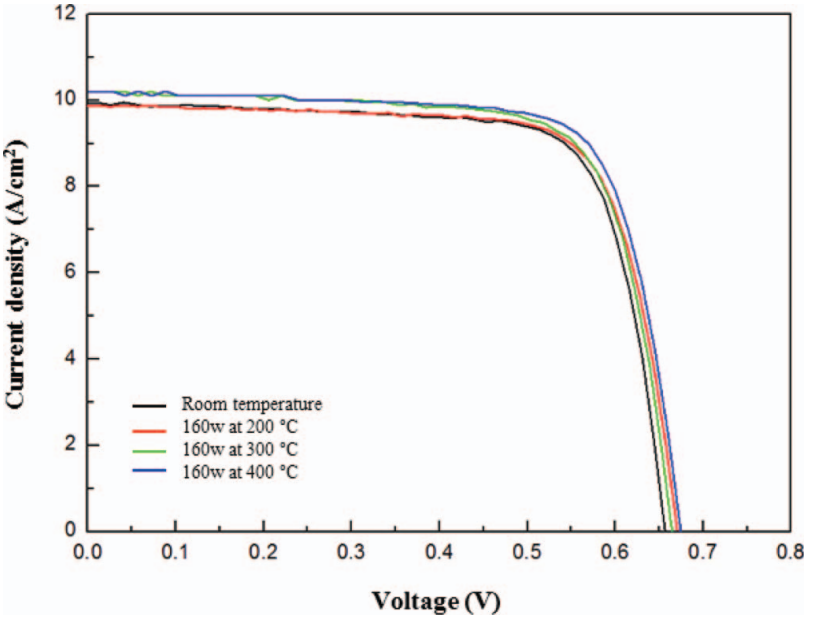

Figure 8. The photocurrent and voltage curves of the DSSCs prepared at various temperatures.

power of the TiO_2 passivating layer for control thickness should be lower than 200 W. In contrast, a slight increase in transmittance is observed with the increase in substrate temperature, as shown in Fig. 6. The sputtering at room temperature results in the least transmittance, which may be attributed to the light scattering loss for its higher surface roughness.

The most important parameter for a solar cell is its photoelectric conversion efficiency: the ratio of the output power to the incident power. The I-V characteristics of the prepared DSSCs, obtained under simulated sun light (an irradiated power density equal to Ps = 100 mW cm^{-2}) are presented in Fig. 7. For the hybrid TiO_2/TNT 10 wt.% cell, the best results for conversion efficiency were obtained; the cells made purely of TiO_2 nanoparticles showed the worst results for conversion efficiency. The DSSCs made of TNT/TiO_2 nanoparticles hybrids showed better photovoltaic performance than cells made purely of TiO_2 nanoparticles. The DSSC prepared without a passivating layer had a short-circuit

Table 1. The photovoltaic performances of the DSSCs prepared at different RF powers and without TNTs.

	Voc (V)	Jsc (mA/cm^2)	FF (%)	η (%)
Without passivating layer (without TNT)	0.66	8.66	66.8	3.84
Without passivating layer (TiO_2/TNT)	0.66	8.58	74.9	4.31
RF power at 80 W (TiO_2/TNT)	0.65	9.29	75.1	4.57
RF power at 120 W (TiO_2/TNT)	0.66	9.75	73.4	4.76
RF power at 160 W (TiO_2/TNT)	0.65	9.93	74.8	4.89
RF power at 200 W (TiO_2/TNT)	0.66	9.40	75.0	4.72

Table 2. The photovoltaic performances of the DSSCs prepared at different substrate temperatures.

	Voc (V)	Jsc (mA cm^{-2})	FF (%)	η (%)
Room temperature (RF power 160 W)	0.65	9.93	74.8	4.89
Substrate temperature 200°C (RF power 160 W)	0.67	9.85	74.7	4.93
Substrate temperature 300°C (RF power 160 W)	0.66	10.18	73.8	4.99
Substrate temperature 400°C (RF power 160 W)	0.67	10.18	74.7	5.12

current density (Jsc) of 8.58 A cm^{-2}, an open-circuit potential (Voc) of 0.66 V, and a cell conversion efficiency of 4.31%. The DSSC fabricated with the TiO_2 passivating layer sputtered at 5 mTorr, 160 W, shows the highest efficiency (4.89%) value, due to the decreased conductivity of electrons from the nanoporous TiO_2 layer to the FTO electrode. The increase in the thickness of the the TiO_2 passivating layer by increasing the RF power resulted in a decreased efficiency of the RF power at 200 W (4.76%) due to a decreased conductivity of electrons from the nanoporous TiO_2 layer to the FTO electrode.

Figure 8 shows the photocurrent-photovoltage characteristics of the solar cells with the TiO_2 passivating layer sputtered at room temperature, 200°C, 300°C, and 400°C at RF power of 160 W. In this work, a slight increase in the transmittance and in the efficiency are observed with the increase in substrate temperature. Tables 1 and 2 summarize the detailed performances of the fabricated DSSCs. Although the insertion of the TiO_2 passivating layer increases the efficiency by effective prevention of electron transfer from the FTO electrode to the electrolyte, the decreased fill factor (FF) value demonstrated the decreased conductivity of the FTO electrode covered by the TiO_2 passivating layer. Therefore, considering the effective passivation and high conductivity and transmittance of the FTO electrode simultaneously, it is necessary to optimize the thickness and substrate temperature of the TiO_2 passivating layer.

Conclusion

In summary, the characteristics of the RF-sputtered TiO_2 passivating layer at various substrate temperatures and thicknesses at different RF powers on the FTO electrode were investigated for its application in DSSCs. The optical transparency and surface roughness of the TiO_2 passivating layer depend on the RF sputtering conditions. The passivating layer deposited at an RF power of 160 W and a substrate temperature of 400°C shows the best result at 5.12%: a short-circuit current density of 10.18 mA cm^{-2}, an open-circuit voltage of 0.67 V, and an FF of 74.70% was achieved. In addition, The DSSC based on a TiO_2/TNT combination at the optimal weight ratio (TNT 10 wt.%) showed better photovoltaic performance than the cell made purely of TiO_2 nanoparticles. It can be said that the improved conversion efficiency could be associated with the improved specific surface area of the passivating layer.

Acknowledgment

This study was supported by the Human Resources Development of the Korea Institute of Energy Technology Evaluation and Planning (KETEP) grant funded by the Korea government's Ministry of Knowledge Economy (no. 20104010100510).

References

[1] Grätzel, M. (2004). *J. Photochem. Photobiol. A*, *164*, 3.
[2] O'Regan, B., & Grätzel, M. (2004). *Nature*, *353*, 737.
[3] Hamann, T. W., Jensen, R. A., Martinson, F., Ryswyk, H. V., & Hupp, J. T. (2008). *Energ. Environ. Sci.*, *1*, 66.
[4] Kong, F. T., Dai, S.-Y., & Wang, K. J. (2007). *Adv. Opto. Elect.*, *10*, 1–14.
[5] Xia, J., Masaki, N., Jiang, K., Wada, Y., & Yanagida, S. (2006). *Chem. Lett.*, *35*, 252.
[6] Ito, S., Liska, P., Comte, P., Charvet, R., Péchy, P., Bach, U., Schmidt-Mende, L., Zakeeruddin, S. M., Kay, A., Nazeeruddin, M. K., & Grätzel, M. (2005). *Chem. Commun.*, 4351.
[7] Peng, B., Jungmann, G., Jäger, C., Haarer, D., Schmidt, H.-W., & Thelakkat, M. (2001). *Coord. Chem. Rev.*, *248*, 1479.
[8] Paulose, M., Shankar, K., Varghese, O. K., Mor, G. K., Hardin, B., & Grimes, C. A. (2006). *Nanotechnology*, *7*, 1446.
[9] Mor, G. K., Varghese, O. K., Paulose, M., Shankar, K., & Grimes, C. A. (2006). *Sol. Energy Mater. Sol. Cells*, *90*, 2011.
[10] Cameron, P. J., & Peter, L. M. (2004). *J. Phys. Chem. B*, *107*, 14394.
[11] Karthikeyan, C. S., Thelakkat, M., & Willert-Porada, M. (2006). *Thin Solid Films*, *511*(18), 7.
[12] Hattori, R., & Goto, H. (2007). *Thin Solid Films*, *515*, 8045.
[13] Anpo, M., & Chiba, K. (1992). *J. Mol. Catal. 74*, 207.
[14] Jin, Y. S., Kim, K. H., Kim, W. J., Jang, K. U., & Choi, H. W. (2011). *Ceram Int.*, *38*, S505–S509.
[15] Lee, C. H., Kim, K. H., Jang, K. U., Park, S. J., & Choi, H. W. (2011). *Mol. Cry. Liq. Cry.*, *539*, 125.
[16] Ito, S., Chen, P., Comte, P., Nazeeruddin, M. K., Liska, P., Pechy, P., & Grätzel, M. (2007). *Prog. Photovolt. Res. Appl.*, *15*, 603.
[17] Jeong, J. A., & Kim, H. K. (2011). *Sol. Energy Mater. Sol. Cells*, *95*, 344.